RESEARCH ARTICLE | JUNE 12 2023

# Non-covalent interactions involving $\pi$ effect between organic cations in low-dimensional organic/inorganic hybrid perovskites $\odot$

Liang Yan ■ <sup>(a)</sup>; Camryn J. Gloor <sup>(b)</sup>; Andrew M. Moran <sup>(b)</sup>; Wei You ■ <sup>(c)</sup>



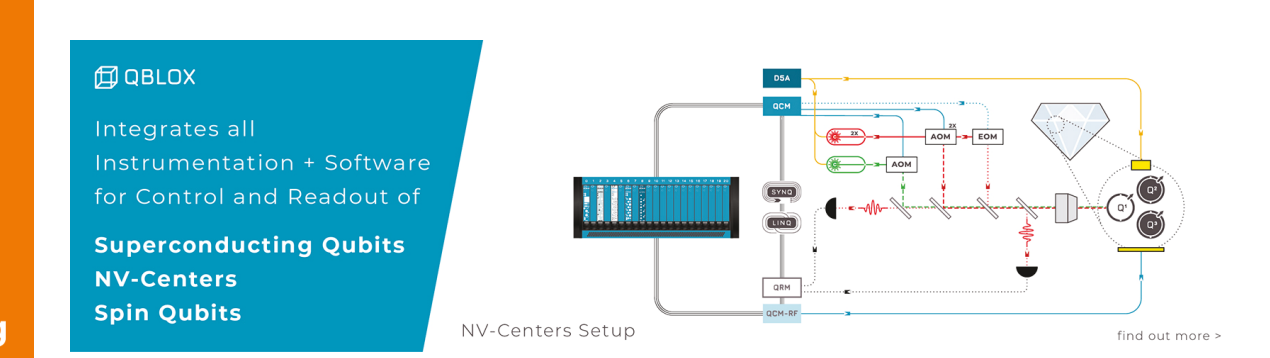
Appl. Phys. Lett. 122, 240501 (2023) https://doi.org/10.1063/5.0148876





Citation

CrossMark





## Non-covalent interactions involving $\pi$ effect between organic cations in low-dimensional organic/inorganic hybrid perovskites 🐵

Cite as: Appl. Phys. Lett. 122, 240501 (2023); doi: 10.1063/5.0148876 Submitted: 2 March 2023 · Accepted: 21 May 2023 · Published Online: 12 June 2023







Liang Yan, (a) (b) Camryn J. Gloor, (b) Andrew M. Moran, (b) and Wei You (b)



#### **AFFILIATIONS**

Department of Chemistry, University of North Carolina at Chapel Hill, Chapel Hill, North Carolina 27599, USA

<sup>a)</sup>Authors to whom correspondence should be addressed: lyan1@live.unc.edu and wyou@unc.edu

#### **ABSTRACT**

Low-dimensional organic/inorganic hybrid perovskites (OIHPs) are a promising class of materials with a wide range of potential applications in optoelectronics and other fields since these materials can synergistically combine individual features of organic molecules and inorganics into unique properties. Non-covalent interactions are commonly observed in OIHPs, in particular, π-effect interactions between the organic cations. Such non-covalent interactions can significantly influence important properties of the low-dimensional OIHPs, including dielectric confinement, bandgap, photoluminescence, quantum efficiency, charge mobility, trap density, stability, and chirality. This perspective reviews recent studies of non-covalent interactions involving the  $\pi$  systems of organic cations in low-dimensional OIHPs. The analysis of crystal structures of low-dimensional OIHPs offers significant insight into understanding such non-covalent interactions and their impacts on specific properties of these OIHPs. The developed structure-property relationships can be used to engineer non-covalent interactions in low-dimensional OIHPs for applications.

Published under an exclusive license by AIP Publishing. https://doi.org/10.1063/5.0148876

#### I. INTRODUCTION

Organic-inorganic hybrid halide perovskites (OIHPs) have attracted growing attention in the past decade due to their peculiar (optoelectronic) properties that can be utilized for applications, such as photovoltaics (PV), light-emitting diodes, and detectors. 1-4 Threedimensional (3D) OIHPs are the most widely studied systems that have a general chemical formula of AMX3; structurally, 3D OIHPs are a 3D network of corner-sharing metal (M, e.g., Pb<sup>2+</sup>) halide (X) octahedra, in which A<sup>+</sup> is typically an organic cation occupying the 12-fold coordinated sites between the octahedra. However, when the organic cations are too large to form stable 3D OIHPs, lowdimensional OIHPs would form accordingly [Fig. 1(a)], including two-dimensional (2D), one-dimensional (1D), and zero-dimensional (0D), categorized based on how the inorganic corner shared octahedra are assembled. In 2D OIHPs, the octahedra are assembled into layers, which could be considered as the 3D OIHPs cut from different crystal planes. Specifically, slicing 3D OIHPs from their (100) plane can form the Ruddlesden-Popper (RP) phase, Dion-Jacobson (DJ) phase, and alternating cations in the interlayer space (ACI phase); however, (110)-oriented corrugated perovskites and (111)-oriented defective perovskites also exist (Fig. 1). On the other hand, the inorganic

octahedra are assembled into lines or chains in 1D OIHPs,5 whereas dots or clusters are found in 0D OIHPs.6

In all these low-dimensional perovskites, as the inorganic octahedra would be low in dimension, there would be a strong quantum confinement effect; furthermore, the dielectric difference between organic and inorganic parts would lead to the dielectric confinement effect, 8-10 leading to strong excitonic effects in low-dimensional OIHPs. One of the main advantages of low-dimensional organic/inorganic hybrid perovskites is their tunable optoelectronic properties, which can be manipulated by changing the size, shape, and arrangement of the organic and inorganic components. Furthermore, one outstanding challenge for 3D OIHPs is their stability to moisture, heat, and light; 11 by contrast, lowdimensional OIHPs exhibit much better stability. 12,13 This high level of tunability and stability bode well for a wide range of applications, including solar cells, light emitting diodes (LEDs), sensors, and other optoelectronic devices. 12,13 Finally, these low-dimensional OIHPs can be synthesized with a variety of solution-based and vapor-based techniques<sup>14</sup> and can also be fabricated with a wide range of processing methods, including spin-coating, printing, and other techniques.<sup>14</sup>

Structurally, the organic molecules/cations in between the assemblies (layers, lines, or dots) of inorganic octahedra have at least one

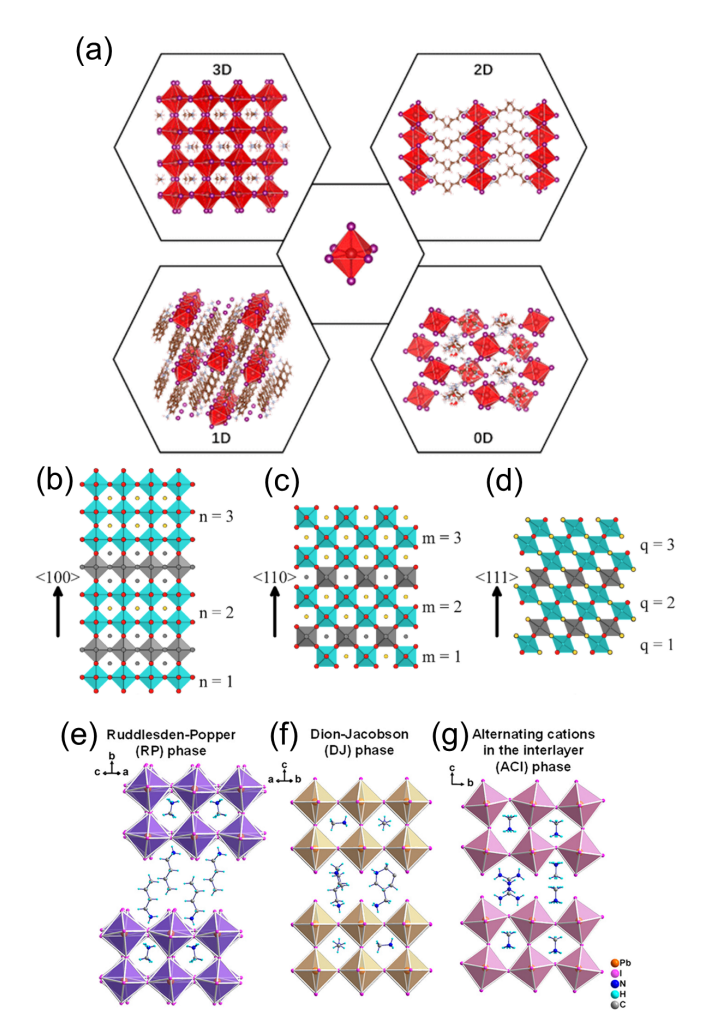
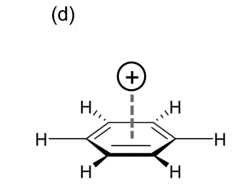


**FIG. 1.** (a) Scheme of a typical 3D perovskite structure and the derived low-dimensional cases [adapted with permission from Lyu *et al.*, J. Am. Chem. Soc. **143**(32), 12766 (2021). Copyright 2021 American Chemical Society]. <sup>15</sup> 2D perovskites scheme for (b)  $\langle 100 \rangle$ , (c) $\langle 110 \rangle$ , and (d)  $\langle 111 \rangle$  orientated 2D perovskites [adapted with permission from B. Saparov and D. B. Mitzi, Chem. Rev. **116**(7), 4558 (2016). Copyright 2016 American Chemical Society], <sup>16</sup> scheme for typical (e) RP, (f) DJ, and (g) ACI phases of 2D perovskites [adapted with permission from Li *et al.*, Chem. Rev. **121**(4), 2230 (2021). Copyright 2021 American Chemical Society]. <sup>17</sup>

ammonium cation that connects with inorganic octahedra via ionic interactions; in addition, hydrogen bonds also exist between the hydrogen atom in ammonium and the halogen atoms in inorganic octahedra. On the other hand, especially for the monoammonium cation-based perovskites, the non-covalent interactions (e.g., van der



Waals forces) between these organic molecules hold multiple hybrid assemblies into the bulk material, which could change the formation energy of the low-dimensional OIHPs. These non-covalent interactions (between organic cations) can be categorized into (a) nonelectrostatic interactions, including van der Waals forces,  $\pi$ -effect interactions, and hydrophobic effect, and (b) electrostatic interactions, including ionic interactions, hydrogen bonding, and halogen bonding. We will focus on the  $\pi$ -effect interactions since such interactions previously exclusively studied in organic and supramolecular chemistry community<sup>18</sup>—have recently emerged as important tools in tuning the structure and properties of low-dimensional perovskites. 19-27 In fact, coupling with known organic molecules that can provide extra functionalities (e.g., light-absorbing, chirality, enhancing conductivity, manipulating band alignments, and suppressing halide ion diffusion),  $\frac{19,20,28-37}{19,20,28-37}$  the  $\pi$ -effect interactions can enable functional lowdimensional perovskites with unique properties.

### II. $\pi$ -EFFECT INTERACTIONS IN LOW-DIMENSIONAL PEROVSKITES

Non-covalent  $\pi$ -effect interactions are promoted by delocalized  $\pi$  electron systems in conjugated organic molecules (e.g., benzene). Depending upon the species involved,  $\pi$ -effect interactions include the  $\pi$ - $\pi$  interactions (stacking), ion- $\pi$  interactions (cation- $\pi$  and anion- $\pi$  interaction), XH  $\cdots$   $\pi$  interactions (such as CH $\cdots$  $\pi$  interaction), among others. Figure 2 presents several typical  $\pi$ -effect interactions and how they impact the molecular stacking.

 $\pi$ - $\pi$  interactions (stacking) represent the dispersion force arising from van der Waals forces between aromatic organic molecules. The majority of  $\pi$ - $\pi$  interactions (stacking) exhibit energies within the range of -0.5 to -2.0 kcal  $\mathrm{mol}^{-1.38}$  However, arylperfluoroaryl interactions represent a unique case of  $\pi$ - $\pi$  interactions (stacking) with stronger couplings. For instance, when benzene is fully substituted with fluorine (i.e., perfluorobenzene), the quadrupole moment reverses direction when compared to that of benzene, resulting in a strong co-facile interaction between perfluorobenzene and benzene. Attributable to the attractive electrostatic quadrupole-quadrupole interactions and potential CH-F interactions, the aryl-perfluoroaryl interaction energy (e.g., -4.33 kcal  $\mathrm{mol}^{-1}$  between benzene and hexafluorobenzene)<sup>39</sup> can be on the same order as that of hydrogen bonds.

The primary driving force of cation– $\pi$  interactions is electrostatics, but induction and dispersion can also contribute significantly, especially in the case of larger organic cations. <sup>40</sup> Cation– $\pi$  interactions typically exhibit energies ranging from -2 to -4 kcal mol<sup>-1</sup>, and for certain metal cation– $\pi$  interaction pairs, the energies can reach between -6 and -13 kcal mol<sup>-1,38</sup>

A significant characteristic of the CH $\cdots\pi$  interaction is that the dispersion energy dominates in cases where  $sp^3$ - and  $sp^2$ -CHs are involved as the hydrogen donor, with minimal contribution from

**FIG. 2.** Four typical  $\pi$ -effects interactions: (a) aryl–perfluoroaryl interaction, (b)  $\pi$  donor–acceptor interactions, (c)  $\text{CH} \cdots \pi$  interactions, and (d) cation– $\pi$  interactions.

**FIG. 3.** Plausible  $\pi-\pi$  stacking configuration: (a) T-shaped, (b) parallel-displaced, and (c) sandwich.

electrostatics. In typical scenarios, where aliphatic and aromatic CH groups are involved as the hydrogen donor, the energy of CH $\cdots\pi$  interaction ranges from approximately -1.5 to -2.5 kcal mol $^{-1}$ , which is smaller than the cation $-\pi$  interaction but close to the conventional  $\pi-\pi$  interaction.

Since most  $\pi$ -effect interactions can be deliberately introduced into low-dimensional perovskites by the molecular design of organic cations, the incorporation of  $\pi$ -effect interactions has become an important tool to modulate optoelectronic properties of low-dimensional perovskites and therefore has significant implications for device performance (e.g., efficiency and stability of solar cells). <sup>19,20,25,42</sup>

#### A. $\pi$ - $\pi$ interaction (stacking)

Benzene is the simplest aromatic molecule and has been included in organic cations, such as phenethylammonium (PEA)—one of the most widely studied organic cations for low-dimensional perovskites. <sup>43–47</sup> In the case of PEA, the permanent quadrupole moment of the benzene introduces a positive charge on the ring (i.e., H) and a negative charge above and below the ring. Therefore, T-shaped or parallel-displaced stacking between benzenes is preferred, while a face-to-face sandwiched stacking usually does not occur (Fig. 3). <sup>48</sup> It is rather difficult to determine the stacking of substituted benzenes, since many factors are in play, including the geometry, electrostatics, dispersion, and direct interactions. <sup>49–52</sup>

For PEA-based 2D lead halide perovskites, a typical T-shaped stacking was observed,  $^{53}$  which could be induced by the  $sp^2$  CH··· $\pi$  interaction.  $^{54}$  However, when PEA is functionalized with a single fluorine atom at different positions (ortho, meta, or para), the relative packing arrangement of F-substituted PEA in 2D lead halide perovskites is different from the unsubstituted PEA and is dependent upon the substitution position of the fluorine atom, as Hu  $et\,al.$  discovered.  $^{20}$  They synthesized 2D perovskites with a single F-atom-substituted PEA as the organic cation and grew single crystals to further study the structure–property relationship. The crystal structures of 2D perovskites (n = 1) with fluorinated PEA cations [Fig. 4(a)] and the density functional theory (DFT) calculations established the rules for packing of these substituted PEA cations. Importantly, the calculated

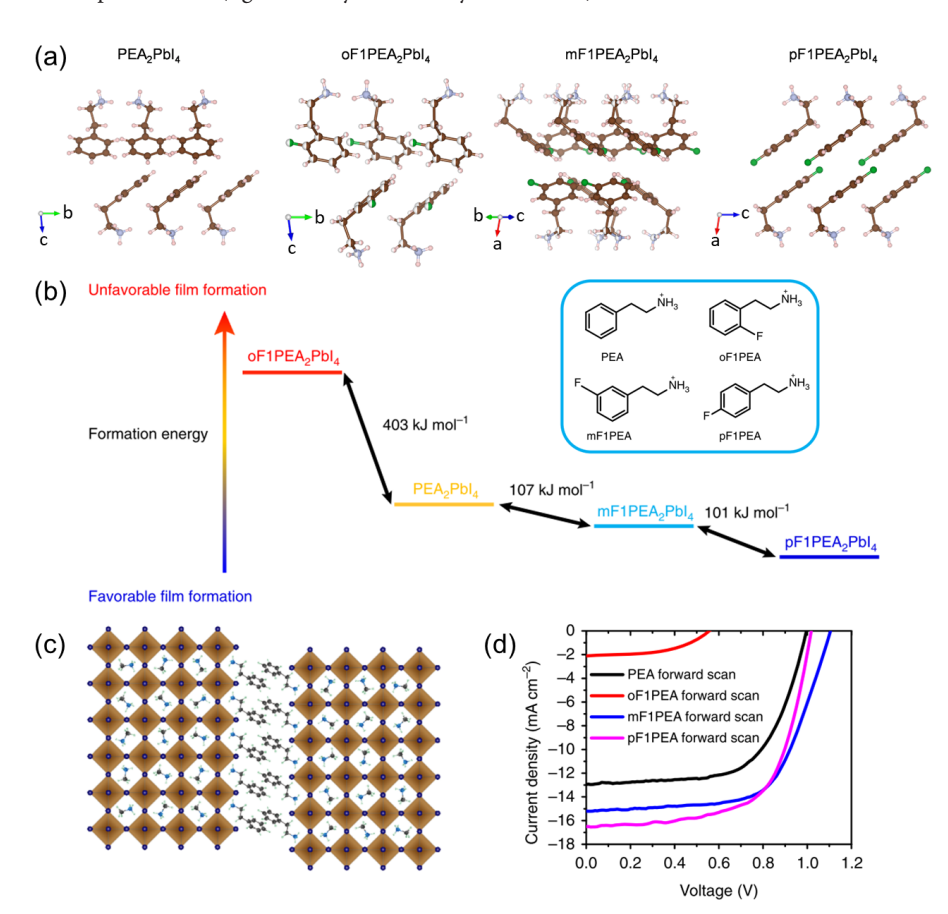


FIG. 4. (a) Idealized crystal structures of 2D perovskite (n = 1) with different cations showing the different packing arrangements within the organic interlayer for PEA (this structure was redrawn based on the work by Du et al.53), oF1PEA, mF1PEA, and pF1PEA. (b) The relative formation energies of these 2D perovskites, with the inset showing the chemical structures of the organic cations. (c) Crystal sketch of PEA based 2D perovskites (n = 4) with PEA fluorinated at different positions. (d) Current-density-voltage (J-V) curves of their photovoltaic devices (forward scan) under 1 sun condition (AM 1.5G) with a solar simulator. Adapted with permission from Hu et al., Nat. Commun. 10(1), 1276 (2019). Copyright 2019 Nature Publishing

formation energies of these 2D perovskites (n = 1) correlated well with variations in packing and disorder of the spacer cations [Fig. 4(b)]. Furthermore, Hu *et al.* demonstrated that the photovoltaic efficiency of 2D perovskites (n = 4) based solar cells [Fig. 4(c)] highly depends on the fluorination position of PEA [Fig. 4(d)]. Specifically, efficiencies greater than 10% were achieved when 3-fluorophenethylammonium (mF1PEA) or 4-fluorophenethylammonium (pF1PEA) was used as the organic cation in such 2D perovskites based solar cells. By contrast, the efficiencies of solar cells based on 2-fluorophenethylammonium (oF1PEA) were less than 1%. It was proposed that a more favorable formation energy and less crystallographic disorder are beneficial for the device performance of these 2D perovskite-based solar cells. The  $\pi$ -effect interaction (through organic cations) was shown to primarily determine the performance of solar cells based on 2D perovskites.

Fluorination of PEA can also lead to a change in the distance between the inorganic layers, thereby tuning the electronic properties, such as out-of-plane mobility; this enhanced mobility was believed to be the leading reason for the much-improved efficiency of 2D perovskites (n = 5) with 4-fluorophenethylammonium (F-PEA) compared to the PEA based counterpart.<sup>27</sup> By analyzing the single-crystal XRD data for each structure [n = 1, F-PEA or PEA only, Figs. 5(a)–5(d)], Zhang *et al.* revealed that the phenyl rings are parallel slip-stacked in the F-PEA based structure [Figs. 5(c) and 5(d)], promoted by the interaction between F-PEA molecules; by contrast, edge-to-face was observed in the PEA structure [Figs. 5(a) and 5(b)]. Importantly, the average phenyl ring centroid—centroid distances in the organic layer became shorter for F-PEA based 2D perovskites. Thus, it is likely that

there is enhanced  $\pi\text{-}\text{orbital}$  overlap in the out-of-plane direction of the aromatic moieties in F-PEA based perovskites relative to PEA based ones, which could facilitate more efficient charge transport. It also appears that the F-PEA cation aligns the stacking of inorganic slabs better. All these structural changes induced by the incorporation of F-PEA in 2D perovskites led to enhanced orbital interactions, improved charge transport across adjacent inorganic layers, increased carrier lifetime, and reduced trap density [Fig. 5(e)], all of which are beneficial for the device performance. Using a simple spin coating deposition technique at room temperature without any additives, F-PEA based perovskite solar cells demonstrated higher efficiency than PEA based cells (for both n = 1 and  $\langle n \rangle$  = 5) [Figs. 5(f) and 5(g)]. Later, Shi et al. also used F-PEA to prepare quasi-2D perovskite ( $\langle n \rangle$  = 5) solar cells and reached 17% efficiency.  $^{42}$ 

In addition to solar cell applications,  $\pi - \pi$  stacking has also been utilized in low-dimensional perovskite-based field effect transistors (FETs).<sup>55,56</sup> Gao *et al.* utilized a large, conjugated cation-based perovskite [(4Tm)<sub>2</sub>SnI<sub>4</sub>] to achieve hole mobility up to 2.32 cm<sup>2</sup> V<sup>-1</sup> s<sup>-1,55</sup> and their tin based 2D perovskites exhibited a dramatic improvement in stability compared to the previous benchmark material, (PEA)<sub>2</sub>SnI<sub>4</sub>.<sup>57</sup> It was found that the strong intermolecular interactions between the organic cations play an important role in increasing the crystal formation energy to achieve large grain sizes in their perovskite films.<sup>55</sup> Furthermore, Liang and Gao *et al.* designed organic cations containing fused-thiophene rings, specifically thienothiophene (TT) and dithienothiophene (DTT) [chemical structures in Figs. 6(a)–6(c)]. Each of these cations could form 2D perovskites, as demonstrated by

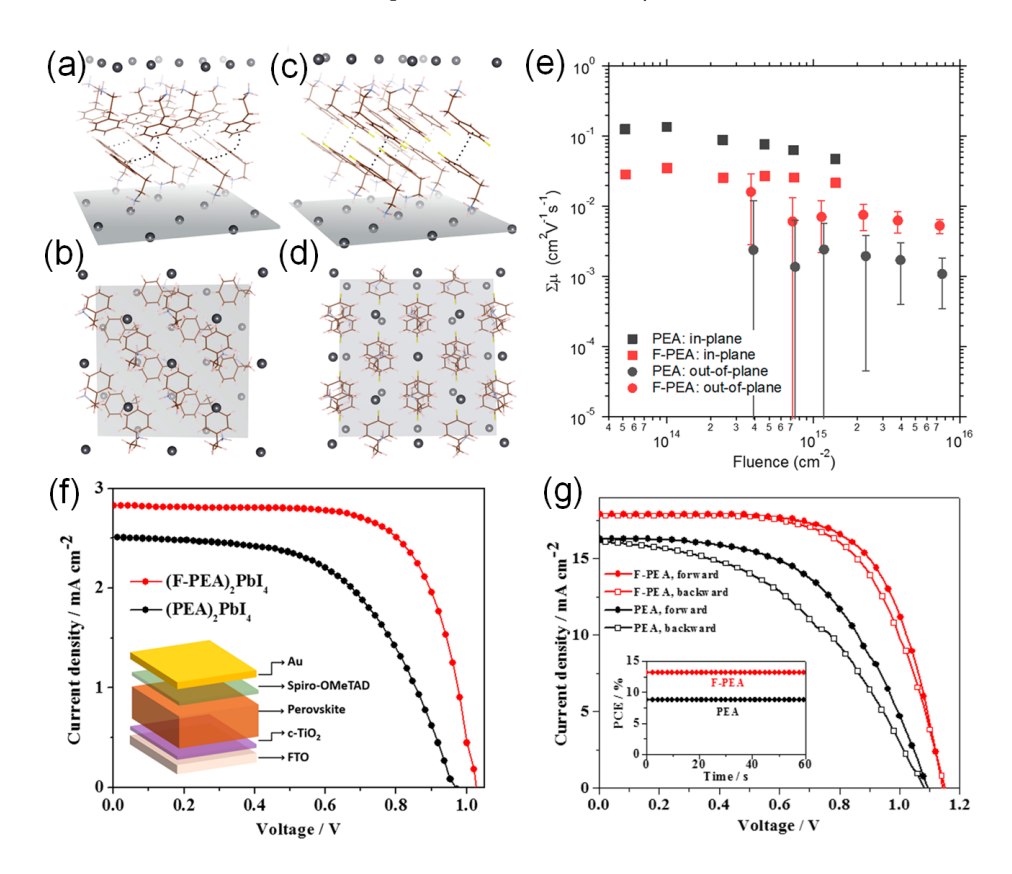
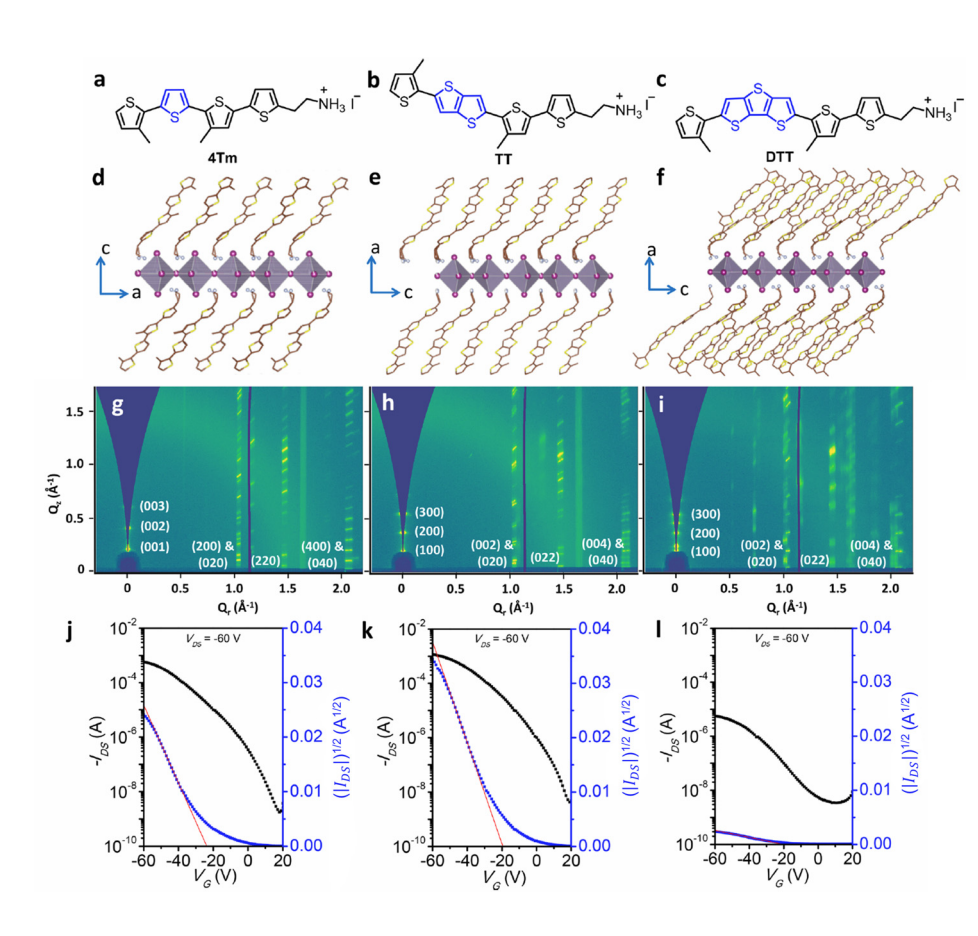


FIG. 5. The structures of (a) and (b) (PEA)<sub>2</sub>PbI<sub>4</sub> and (c) and (d) (F-PEA)<sub>2</sub>PbI<sub>4</sub>single-crystal structures. based Time-resolved microwave conductivity comparison of out-of-plane and in-plane transport for 2D perovskite (n = 1) thin films. (f) J-V curves of perovskite solar cells based on (PEA)2PbI4 and (F-PEA)<sub>2</sub>Pbl<sub>4</sub>. (g) J-V curves of solar cells based on 2D (PEA)<sub>2</sub>MA<sub>4</sub>Pb<sub>5</sub>I<sub>16</sub> and (F- $PEA)_2MA_4Pb_5I_{16}$  (n = 5). Adapted with permission from Zhang et al., J. Am. Chem. Soc. 141, 5972 (2019). Copyright 2019 American Chemical Society.



**FIG. 6.** 2D RP phase halide perovskites featured with conjugated ligands. Chemical structures of the (a)  $4\,\mathrm{Tm}$ , (b) TT, and (c) DTT organic cations. Side view of the crystal structures of (d)  $(4\,\mathrm{Tm})_2\mathrm{Snl}_4$ , (e)  $(TT)_2\mathrm{Snl}_4$ , and (f)  $(DTT)_2\mathrm{Snl}_4$ , GWAXS patterns for thin-film samples of (g)  $(4\,\mathrm{Tm})_2\mathrm{Snl}_4$ , (h)  $(TT)_2\mathrm{Snl}_4$ , and (i)  $(DTT)_2\mathrm{Snl}_4$  on  $Sio_2/\mathrm{Si}$  substates. Transfer characteristics of BG/TC FET devices based on (j)  $(4\,\mathrm{Tm})_2\mathrm{Snl}_4$ , (k)  $(TT)_2\mathrm{Snl}_4$ , and (l)  $(DTT)_2\mathrm{Snl}_4$ . Adapted with permission from Liang et al., J. Am. Chem. Soc. **143**(37), 15215 (2021). Copyright 2021 American Chemical Society.

the crystal structures shown in Figs. 6(d)-6(g). Those organic cations exhibit stronger intermolecular interactions and influence perovskite crystal nuclei formation, which resulted in thin films with highly ordered crystalline structures and extremely large grain sizes. Under optimal conditions, (TT)<sub>2</sub>SnI<sub>4</sub>-based FETs demonstrated the highest

field-effect mobility, reaching up to  $9.35~\rm cm^2~V^{-1}~s^{-1}$  and an ON/OFF current ratio greater than  $10^5$ . These impressive results further underscore the significance of tailoring the rigidity and intermolecular interactions of organic cations in managing 2D perovskite crystallization and thin-film growth to obtain superior properties. <sup>56</sup> Interestingly, the

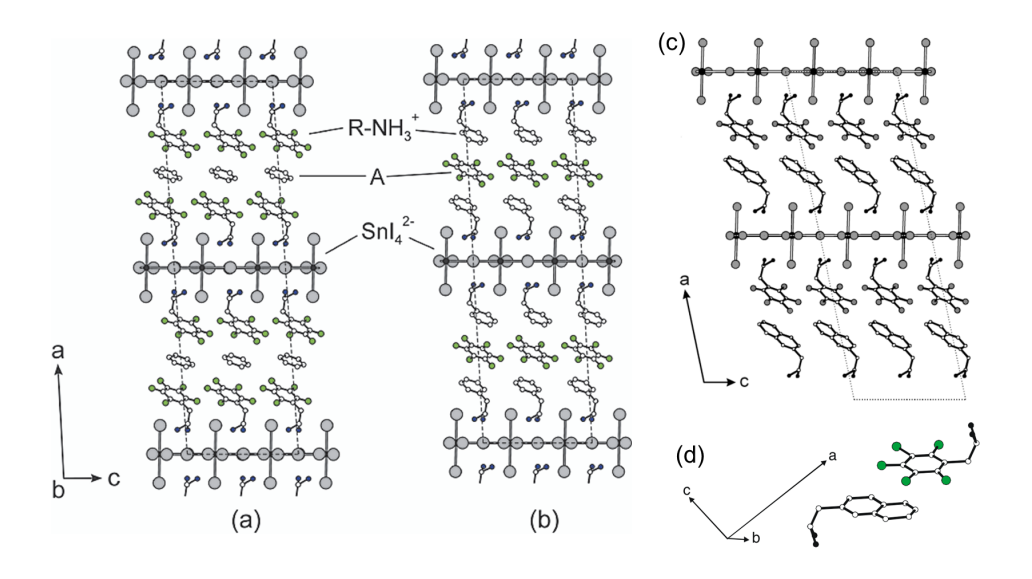


FIG. 7. Aryl-perfluoroaryl interaction in perovskite. Crystal structures of (a)  $(C_6F_5C_2H_4NH_3)_2SnI_4 \cdot C_6H_6$  and (b)  $(C_6H_5C_2H_4NH_3)_2SnI_4 \cdot C_6F_6$ , viewed down the b axis. Dashed lines depict the unit cell outlines. Adapted with permission from Mitzi et al., Inorg. Chem. 41(8), 2134 (2002). Copyright 2002 American Chemical (c) A structural model for the crystal of (F5-PEA • NEA)Snl<sub>4</sub> viewed along the b axis. (d) Face-to-face packing of F5-PEA and NEA in crystal structure. Adapted with permission from Z. Xu and D. B. Mitzi, Chem. Mater. 15(19), 3632 (2003). Copyright 2003 American Chemical Society.

DTT-based 2D perovskite did not exhibit a pure single phase in the thin film, unlike the 4Tm and TT-based 2D perovskites, as evidenced by the additional reflections in the GIWAXS patterns of DTT-based 2D perovskite film compared with those of 4Tm and TT-based 2D perovskite films, as shown in Figs. 6(g)-6(i). DFT calculations also suggested a nearly type II-like band alignment for the DTT-based 2D perovskite, implying suboptimal hole transport in the inorganic layer. Consequently, the DTT-based 2D perovskite FET displayed limited hole mobility compared to the 4Tm and TT-based 2D perovskites [Figs. 6(i)-6(i)].

#### B. Aryl-perfluoroaryl interaction

The aryl–perfluoroaryl interaction is a strong  $\pi$ -effect interaction. For example, aryl-perfluoroaryl interaction can solidify an equimolar quantity of benzene and hexafluorobenzene in an alternating manner at 23.7 °C.58 This strong interaction has been widely used in supramolecular and polymer chemistries; 58-63 however, it was not employed in low-dimensional perovskites until 2002 when Mitzi et al. showed that benzene (C<sub>6</sub>H<sub>6</sub>) or hexafluorobenzene (C<sub>6</sub>F<sub>6</sub>) could intercalate into 2,3,4,5,6-pentafluorophenethylammonium (5F-PEA) or phenethylammonium (PEA) based 2D perovskite, i.e., (C<sub>6</sub>F<sub>5</sub>C<sub>2</sub>H<sub>4</sub>NH<sub>3</sub>)<sub>2</sub>SnI<sub>4</sub> [Fig. 7(a)] or  $(C_6H_5C_2H_4NH_3)_2SnI_4$ , [Fig. 7(b)], respectively.<sup>21</sup> Similar to the structure of the C<sub>6</sub>H<sub>6</sub> • C<sub>6</sub>F<sub>6</sub> complex, the intercalated benzene (C<sub>6</sub>H<sub>6</sub>) or hexafluorobenzene (C<sub>6</sub>F<sub>6</sub>) formed a well-ordered layer into the inorganic framework of 2D perovskites and adopted a face-to-face orientation relative to existing aromatic organic cations with a distance between 3.44 and 3.50 Å, instead of the T shape in pure parent 2D perovskites (with only PEA or F5-PEA). Further thermal analysis of  $(C_6F_5C_2H_4NH_3)_2SnI_4 \bullet C_6H_6$  and  $(C_6H_5C_2H_4NH_3)_2SnI_4 \bullet C_6F_6$  crystals yielded one additional endothermic transition (12.6(5) kJ mol-1 for  $C_6F_5C_2H_4NH_3)_2SnI_4$  •  $C_6H_6$  and 32.1(8) kJ  $mol^{-1}$  for (C<sub>6</sub>H<sub>5</sub>C<sub>2</sub>H<sub>4</sub>NH<sub>3</sub>)<sub>2</sub>SnI<sub>4</sub> • C<sub>6</sub>F<sub>6</sub>, respectively,) with an onset at 145 °C and a weight loss corresponding to the de-intercalation of the intercalated molecule. In 2003, Mitzi and co-workers further demonstrated that the aryl-perfluoroaryl interaction could be directly observed in 2D perovskites between two types of organic cations, i.e., 2,3,4,5,6-pentafluorophenethylammonium (F5-PEA) and 2-naphthyleneethylammonium (NEA) cations [Fig. 7(c)].<sup>24</sup> The idealized crystal structure of (F5PEA • NEA)SnI<sub>4</sub> clearly showed face-to-face packing [Fig. 7(d)] with a distance of 3.36 Å, clearly indicating the aryl-perfluoroaryl interaction.

In 2019, Hu et al. applied the aryl-perfluoroaryl interaction into 2D perovskite solar cells to improve the efficiency and stability. 19 To investigate the interaction among these aromatics, they grew and analyzed the structures of three different 2D perovskite single crystals:  $(PEA)_{2}PbI_{4}$ ,  $(F5-PEA)_{2}PbI_{4}$ , and  $((PEA)_{0.5}(F5-PEA)_{0.5})_{2}PbI_{4}$ , as shown in Fig. 8. The crystal structure of ((PEA)<sub>0.5</sub>(F5-PEA)<sub>0.5</sub>)<sub>2</sub>PbI<sub>4</sub> is disordered, in which the two different cations lay on top of one another [Figs. 8(c) and 8(d)]—a feature which had been previously reported by Mitzi and co-workers. 21,24 Importantly, the herringbone packing in 2D perovskites [Fig. 8(d)] permits two cations (PEA and F5-PEA) to interact in an offset face-to-face or partially eclipsed manner [inset Fig. 8(d)]. 24,64,65 Though the interaction between the PEA and F5-PEA could not be explicitly observed due to the random mixing of PEA and F5-PEA within the structure, this face-to-face packing motif was not observed in PEA only or F5-PEA only based 2D perovskites [see the crystal structures of (PEA)<sub>2</sub>PbI<sub>4</sub><sup>53</sup> and (F5-PEA)<sub>2</sub>PbI<sub>4</sub> in Figs. 8(a), 8(b), 8(e), and 8(f)], even in the presence of disorder.

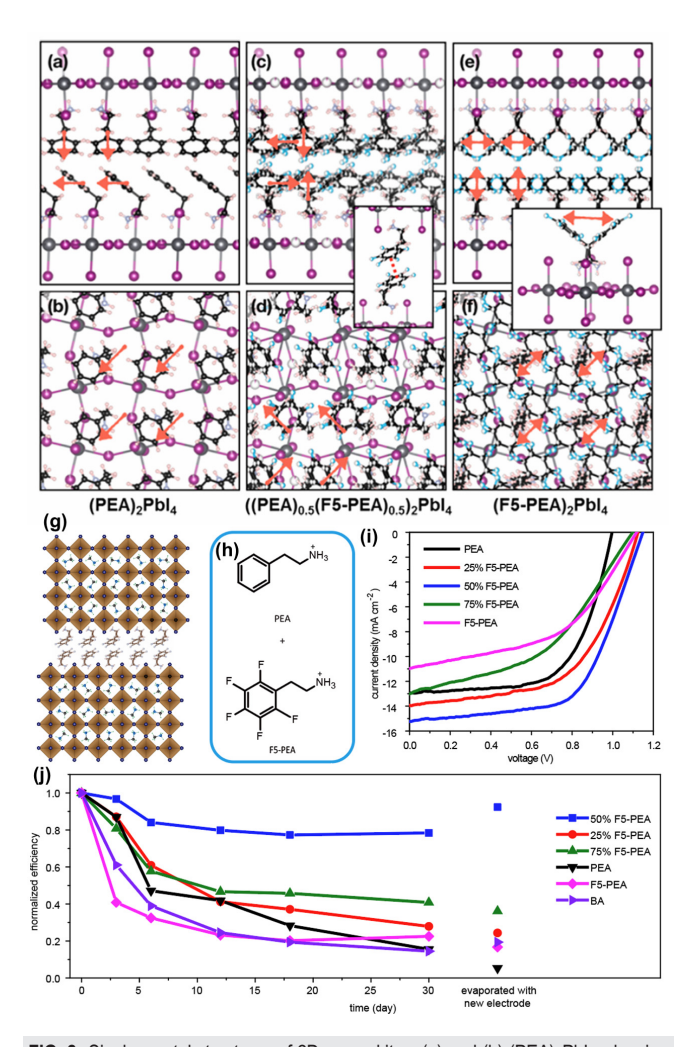


FIG. 8. Single crystal structures of 2D perovskites: (a) and (b) (PEA)<sub>2</sub>Pbl<sub>4</sub>, showing the collinear packing of PEA molecules (this structure was re-drawn based on the work reported by Du et al.<sup>53</sup>), and (c) and (d) ((PEA)<sub>0.5</sub>(F5-PEA)<sub>0.5</sub>)<sub>2</sub>Pbl<sub>4</sub>, showing the herringbone packing of the organic molecules, which are randomly substituted on the same site. The inset highlights the offset face-to-face packing of a pair of organic cations. (e, f) (F5-PEA)<sub>2</sub>Pbl<sub>4</sub>, showing the collinear packing of 5F-PEA, which does not permit face-to-face interactions. The inset shows the equally occupied and disordered orientations of 5F-PEA; occupancy of either orientation leads to a collinear packing of the molecules that does not permit face-to-face interactions. Arrows denote the vector of the +NH<sub>3</sub>CH<sub>2</sub>CH<sub>2</sub>-aryl bond. 2D perovskites and characterization of their photovoltaic devices: (g) crystal sketch of PEA based 2D perovskite (n = 4); (h) molecular structures of PEA and F5-PEA; (i) current-density-voltage (J-V) curves (forward scan) under 1 sun condition (AM 1.5G); and (j) stability of unencapsulated 2D perovskite solar cells for 30 days under 45% relative humidity. Last data point represents the same device after 30 days but with freshly reevaporated electrode. 19 Adapted with permission from Hu et al., ACS Mater. Lett. 1(1), 171 (2019). Copyright 2019 American Chemical Society.

These results highlight the pivotal role of the quadrupole–quadrupole interaction to create this co-facile packing motif in the case of ((PEA)<sub>0.5</sub>(F5-PEA)<sub>0.5</sub>)<sub>2</sub>PbI<sub>4</sub>. With the aryl–perfluoroaryl interaction between PEA and F5-PEA providing additional "adhesion" among organic cations (among other benefits), 2D perovskite solar cells

 $[\langle n\rangle=4,$  Fig. 8(g)] with a 1:1 mix PEA and F5-PEA [structures shown in Fig. 8(h)] achieved the highest efficiency of over 10% [Fig. 8(i)] and the highest device stability [Fig. 8(j)]. This work provides a good example of when tuning the interactions of organic cations via molecular engineering has a profound effect on the device performance and stability of 2D perovskite solar cells.

#### C. $CH \cdots \pi$ interaction

In addition to  $\pi$ – $\pi$  interactions, the CH $\cdots\pi$  interaction is another important interaction that concerns aromatics [see Fig. 2(c)]. Although it is weaker than the aryl–perfluoroaryl interaction or cation– $\pi$  interaction, it is still important in various fields of chemistry, in particular, three-dimensional structure of proteins and DNA. <sup>41</sup>

In 2020, Yan *et al.* reported that the  $CH\cdots\pi$  interaction [Fig. 9(a)] between PEA and propyl ammonium (C3A) affects the device performance of the 2D perovskites solar cell.<sup>25</sup> From both the absorption spectrum and XRD pattern of the mixed cation perovskites with different ratios of C3A vs PEA, Yan *et al.* found that 50% C3A substitution (i.e., C3A:PEA = 1:1) has a distinctively different exciton peak and XRD pattern compared with those of 0% and 100% C3A (i.e., pure PEA and pure C3A based perovskite film of n = 1, respectively), indicating the presence of a third 2D perovskite phase for C3A:PEA = 1:1, likely due to the interaction between C3A and PEA in the organic interlayer. The third phase from the C3A:PEA = 1:1 base 2D perovskite film (n = 1) was also observed from the 25% C3A based film, which has two peaks in its absorption spectrum and XRD pattern,

appearing to be the superposition of the C3A:PEA = 1:1 phase and pure PEA phase. Further evidence for the proposed  $\text{CH} \cdots \pi$  interaction in the 2D perovskites was provided from the Fourier-transform infrared (FTIR) study of these perovskite films (n = 1), as shown in Fig. 9(d). The sp<sup>3</sup> C-H stretching band for the methyl group in C3A (based perovskite film) shifts from 2970 cm<sup>-1</sup> (for pure C3A) to 2963 cm<sup>-1</sup> (for C3A:PEA = 1:1),<sup>66</sup> indicating the  $sp^3$  CH··· $\pi$  interaction between the methyl group in C3A and the benzene ring in PEA. On the other hand,  $sp^2$  C-H stretching located at 3019 cm<sup>-1</sup> for the benzene ring in the PEA based perovskite film almost disappears for the C3A:PEA = 1:1 based film, indicating that the intermolecular CH $\cdots$  $\pi$ interaction between the methyl group in C3A and the benzene  $\pi$  ring in PEA largely replaced the previously existing PEA-PEA ( $sp^2$  CH··· $\pi$ ) interaction in pure PEA based perovskites. This  $sp^3$  CH $\cdots\pi$  interaction could lead to a difference in formation energies for 2D perovskites (n = 1) based on PEA and mixed spacer cations. It was also found that tuning  $CH \cdots \pi$  interaction could have multiple beneficial impacts on such modified 2D perovskites based solar cells, including (i) the removal of the undesirable n = 1 phase, (ii) lowering the density of trap states, and (iii) achieving larger crystalline grains.<sup>25</sup> All of these factors contributed to the observed ~10% efficiency of 1:1 C3A:PEA based 2D perovskite solar cells ( $\langle n \rangle = 3$ ), a 30% increase over pure PEA or pure C3A based ones [Fig. 9(e)]. Additionally, when substituted with 50% C3A, other aromatic ammonium cation [Fig. 9(g)] based 2D perovskites ( $\langle n \rangle = 3$ ) exhibited a similar efficiency enhancement in photovoltaic devices, as shown in Fig. 9(f), indicating the broad applicability of such CH $\cdots$  $\pi$  interactions in 2D perovskites.

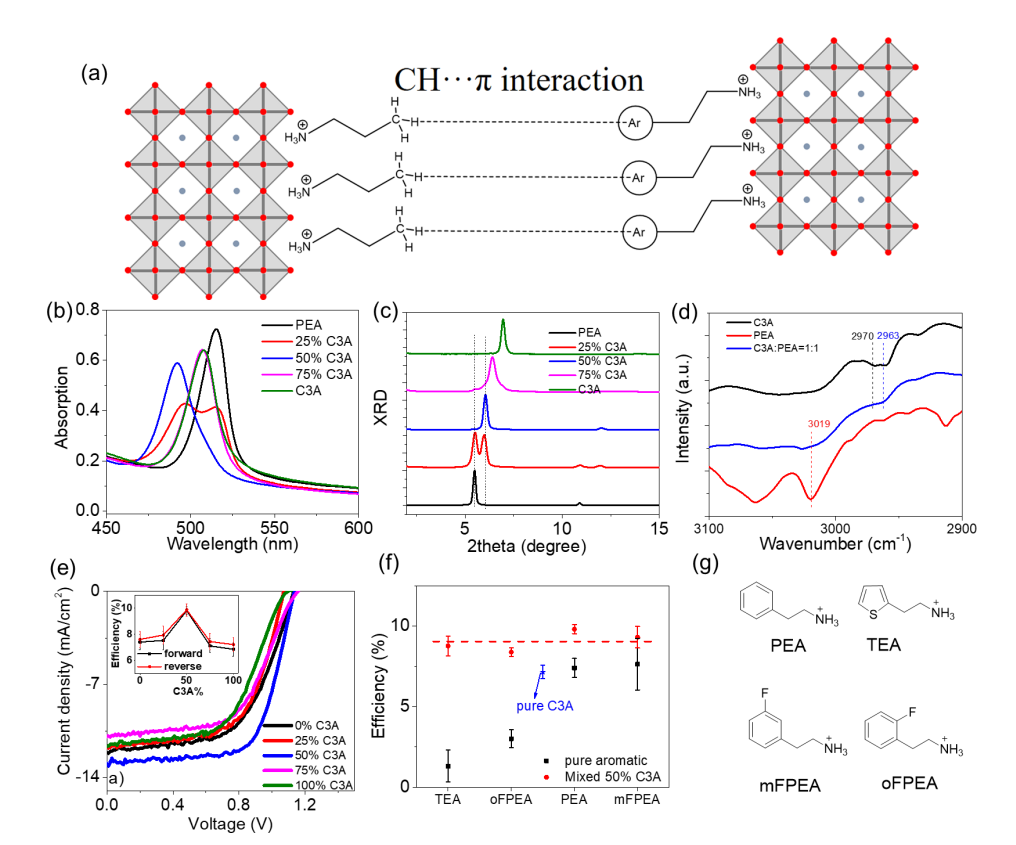


**FIG. 9.** (a) Proposed CH $\cdots\pi$  interaction in 2D hybrid perovskites. (b) Absorption and (c) XRD of mixed PEA:C3A 2D perovskite. (d) FTIR spectrum of pure PEA, pure C3A, and mixed C3A:PEA perovskite. (e) J-V curves of photovoltaic devices based on studied 2D perovskites; the inset is the C3A concentration dependent efficiency. (f) Photovoltaic efficiency enhancement of 2D perovskites with  $\langle n \rangle = 3$  for PEA, oF1PEA, mF1PEA, and TEA after substituting 50% C3A. (g) The chemical structures of these aromatic ammoniums are also listed. Adapted with permission from Yan et al., Sol. RRL 4(1), 1900374 (2020). Copyright 2020 Wiley.

The CH $\cdots\pi$  interaction was also used to adjust the mechanical properties of 2D perovskites.<sup>67</sup> Tu et al. introduced an organic spacer molecule with a rigid phenyl group to form interfaces between the adjacent organic cation layers with  $CH \cdots \pi$  interactions, resulting in high resistance of such 2D perovskites to mechanical deformations. Furthermore, it has been demonstrated that the CH $\cdots\pi$  interaction can be leveraged to enable pure blue emission with 2D perovskites by removing undesirable n = 1 phase.<sup>68</sup> In this study, Tam *et al.* investigated the impact of chain length of alkylammonium in phenyl-alkyl spacer cations on the phase distribution in quasi-2D RP perovskites (n = 2 stoichiometry). They discovered that increasing the alkyl chain length suppresses the formation of the n = 1 phase, which is attributed to a change in the packing arrangement of spacer cations from parallel (in the case of one and two carbon atom alkyl chains) to non-parallel (in the case of three carbon atom alkyl chains). This difference in the packing arrangement is ascribed to weaker  $\pi$ - $\pi$  interactions and enhanced  $CH\cdots\pi$  interactions in perovskite with three carbon atom alkyl chain based alkylammonium cations. A single blue emission peak corresponding to the n=3 phase (466 nm) and n=2 phase (436 nm) was observed in the photoluminescence (PL) spectra of phenylpropylammonium (three carbon atom alkyl chains, PPA) quasi-2D perovskites with methylammonium (MA) and formamidinium (FA) cations, respectively. As a result, efficient sky-blue LEDs with the highest external quantum efficiency (EQE) of 3.35% are achieved for PPA<sub>2</sub>MAPb<sub>2</sub>Br<sub>7</sub> perovskite.<sup>61</sup>

Yan *et al.* further explored the CH $\cdots\pi$  interaction in mixed cation perovskites with chiral cations. The single crystal structures of bromide-based 2D perovskites (n = 1) with 1:1 mixed achiral alkyl cation [e.g., propyl ammonium (C3A) or butyl ammonium (C4A)] and chiral cation [e.g., (R/S  $\beta$ -methylphenethylammonium, R/S MePEA)], exhibit an alternating alkyl cation and chiral cation stacking in between the inorganic slabs [Figs. 10(a) and 10(b)]. In both of the crystal structures, there are very short distances between the H atom and C atom in the benzene ring, 2.847 Å in [S-MePEA][C3A]PbBr<sub>4</sub> and 2.845 Å in [S-MePEA][C4A]PbBr<sub>4</sub>, as shown in Figs. 10(c) and 10(d). All these distances are much smaller than the maximally allowed distance to have such CH $\cdots\pi$  interactions (3.05 Å, 1.05 times of the sum of the van der Waals radii of the H atom in the CH and C atoms in the aromatic ring, i.e.,  $\pi$  system), indicating the presence of CH $\cdots$  $\pi$ interactions. However, there are subtle differences; in the case of [S-MePEA][C3A]PbBr<sub>4</sub>, the CH $\cdots\pi$  interaction is between the terminal CH<sub>3</sub> of the C3 alkyl cation and the  $\pi$  face of the benzene in the S-MePEA cation; by contrast, in the case of [S-MePEA][C4A]PbBr<sub>4</sub>, the  $CH \cdot \cdot \cdot \pi$  interaction switches to between the  $sp^3$  CH of the methyl group at the chiral center of one S-MePEA cation and the  $\pi$  face of the benzene in another S-MePEA cation.

The absorption spectrum of the pure chiral perovskite (i.e., with S/R-MePEA) exhibits a blue-shifted exciton peak, the achiral perovskite (i.e., C4A) possesses a red-shifted peak, and the exciton peak for the mixed-cation perovskite falls in between, as shown in Fig. 10(e). The relative exciton peak energies are consistent with the observed trend in [PbBr<sub>6</sub>] octahedra tilting distortion given by the Pb-Br-Pb bond angles. Interestingly, the mixed-cation perovskites exhibit a circular dichroism (CD) spectrum that is markedly different from that of the pure chiral cation-based analogs. Remarkably, mixed cation perovskites yielded CD signals with greater magnitudes and inverted signs compared to those of pure chiral perovskites at their respective exciton absorption peaks

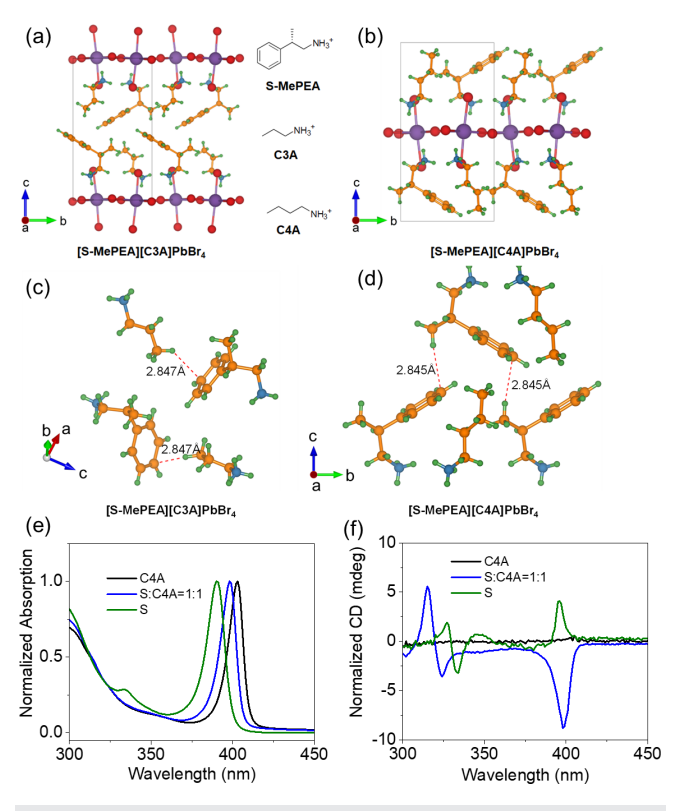


**FIG. 10.** Schematic crystal structures of [S-MePEA][C3A]PbBr<sub>4</sub> (a) and [S-MePEA][C4A]PbBr<sub>4</sub> (b) viewed along the a axis. Pb, Br, C, N, and H atoms are denoted by purple, red, orange, blue, and green spheres, respectively. The chemical structures of the spacer cations, S-MePEA, C3A, and C4A, are shown in the middle. Primary  $sp^3$  CH··· $\pi$  interactions (red dashed lines) in (c) [S-MePEA][C3A]PbBr<sub>4</sub> and (d) [S-MePEA][C4A]PbBr<sub>4</sub> (only organic spacer cations are shown for the structure). (e) Normalized absorption spectra and (f) normalized CD spectra of pure S chiral, pure achiral (C4A) and mixed-cation perovskite films. Adopted with permission from Yan et al, J. Am. Chem. Soc. **143**(43), 18114 (2021). Copyright 2021 American Chemical Society. sl

[Fig. 10(f)]. It was proposed that the symmetry of the crystal structure plays an important role in the amplitude of the CD signal. Specifically, the pure chiral perovskite has a  $P2_12_12_1$  chiral global space group, and the spin polarization from the two individual inorganic layers comprising the unit cell is nearly canceled. On the other hand, the mixed cation perovskites (with space group  $P2_1$ ) contain only one inorganic layer in the unit cell and there is no cancelation of the spin polarization. Therefore, the mixed cation perovskites showed larger CD signals than the pure chiral perovskites. However, the sign inversion and detailed mechanism of CD amplification still needs further theoretical study. Nevertheless, the CH··· $\pi$  interaction plays an important role in stabilizing the mixed cation perovskites and offers alternative avenues for tuning the chiroptical properties of perovskites, instead of solely relying on otherwise complex chemical syntheses of useable chiral cations.

#### D. Cation- $\pi$ interactions

Given the (typical) negatively charged electron cloud of a  $\pi$  system, the positively charged cation can also interact with  $\pi$  systems via

the "cation  $-\pi$  interaction," <sup>69–71</sup> which is essentially an electrostatic interaction in nature. Though cation  $-\pi$  interactions are fundamentally important in understanding the behaviors and properties of molecules in various biological and chemical contexts, <sup>69,70</sup> such interactions were not applied to low-dimensional perovskites until recently. In one example, Sheikh *et al.* discovered that the cation  $-\pi$  interaction helped to achieve water resistant 1D perovskites (e.g., stable in water for 180 days). <sup>22</sup> It was found that 4,4'-trimethylenedipyridine (TMDP) cations are arranged in such a way that the ammonium ions of one TMDP cation are stacked on top of the  $\pi$ -electron rings of the adjacent TMDP cation [Fig. 11(a)]. The distance between the positively charged ammonium ion and the center of the  $\pi$ -electron ring is 3.8 Å, which is the optimal distance to gain the strongest cation  $-\pi$ 

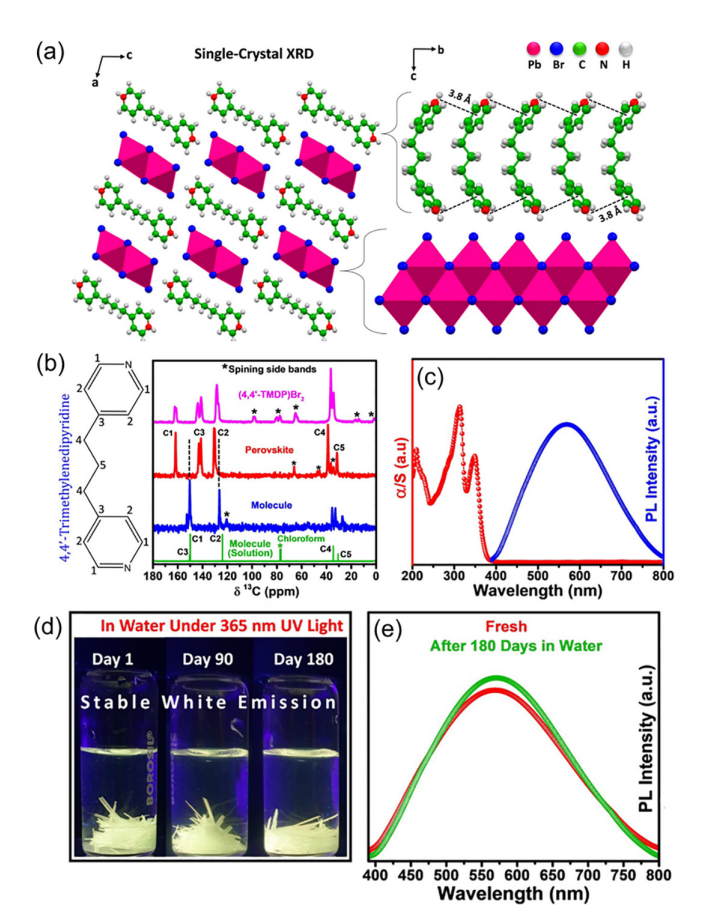


**FIG. 11.** (a) Crystal structure of  $(4,4'\text{-TMDP})\text{Pb}_2\text{Br}_6$  showing cation— $\pi$  stacking: The left panel depicts the crystal structure viewed along the "ac" crystallographic plane, showing edge shared Pb–Br octahedral dimers separated by 4,4'-TMDP cations. The right panel depicts the cation— $\pi$  stacking (shown by dashed black lines) between the 4,4'-TMDP cations along the "b" crystallographic direction and the 1D network of Pb–Br octahedral dimers. (b) NMR spectra revealing the presence of intermolecular cation— $\pi$  interactions in  $(4,4'\text{-TMDP})\text{Pb}_2\text{Br}_6$ . (c) UV–visible absorption (red) and PL (blue) spectra of  $(4,4'\text{-TMDP})\text{Pb}_2\text{Br}_6$ . (d) Photographs of  $(4,4'\text{-TMDP})\text{Pb}_2\text{Br}_6$  crystals in water under 365 nm UV light on day 1, day 90 and day 180 of water treatment. (e) Comparison of the PL spectra of  $(4,4'\text{-TMDP})\text{Pb}_2\text{Br}_6$  before (red) and after (green) the 180 days of water treatment. Adopted with permission from Sheikh et al., Angew. Chem., Int. Ed. 60(33), 18265 (2021). Copyright 2021 Wiley.

interactions. This particular arrangement gives rise to long-range cation- $\pi$  stacking along the b crystallographic axis. The authors further applied the solid state nuclear magnetic resonance (NMR) spectroscopy to investigate the cation –  $\pi$  interaction. The <sup>13</sup>C NMR of TMDP molecule in solution and solid state is quite similar [Fig. 11(b)]; however, for the protonated salt of the TMDP molecule and the 1D perovskite lattice that incorporated the TMDP, the <sup>13</sup>C NMR peaks corresponding to the aromatic carbon atoms changed significantly. These NMR results indicate the presence of cation –  $\pi$  interaction in the solid state of TMDP salt and the corresponding 1D perovskite. Furthermore, the 1D perovskite, (4,4'-TMDP)Pb2Br6, showed broad photoluminescence (PL, blue spectrum) spanning over the entire visible range (400-800 nm) with 365 nm excitation, with a full width at half-maximum (FWHM) of 227 nm [Fig. 11(c)]. The broad emission has the CIE (International Commission on Illumination) chromaticity coordinates of (0.37 and 0.39), corresponding to white light emission. As mentioned earlier, the 1D perovskite is very stable; even after immerging in water for 180 days, the photoluminescence had almost no change compared with the fresh samples as shown in Figs. 11(d) and 11(e). The authors also showed that another 1D perovskite system (4,4'-EDP)Pb<sub>2</sub>Br<sub>6</sub>, where 4,4'-EDP is 4,4'-ethylenedipyridinium ion, exhibited similar cation –  $\pi$  interaction and similar stability and optical properties as those of TMDP based 1D perovskites.

In a more recent work,<sup>23</sup> Sheikh et al. introduced a conjugated bication 4,4'-vinylenedipyridinium (4,4'-VDP), structurally similar to their previously used non-conjugated 4,4'-EDP, in 1D perovskites. The crystal structure of (4,4'-VDP)Pb<sub>2</sub>Br<sub>6</sub> [Fig. 12(a)] is also similar to that of (4,4'-EDP)Pb<sub>2</sub>Br<sub>6</sub>, where the packing of (4,4'-VDP)Pb<sub>2</sub>Br<sub>6</sub> is essentially identical to that of (4,4'-EDP)Pb<sub>2</sub>Br<sub>6</sub>. Both demonstrated very short distances between the positively charged ammonium ion and the center of the  $\pi$ -electron ring [Fig. 12(b)], 3.8 Å for (4,4'-EDP)Pb<sub>2</sub>Br<sub>6</sub> and 3.9 Å for (4,4'-VDP)Pb<sub>2</sub>Br<sub>6</sub>, respectively, indicating the existence of cation –  $\pi$  interaction in both crystal structures. The strong cation –  $\pi$  interaction helps (4,4'-VDP)Pb<sub>2</sub>Br<sub>6</sub> achieve good stability even in water for 1 year with ambient light. Furthermore, due to the  $\pi$ -conjugation throughout the bications 4,4'-VDP, the 1D perovskite (4,4'-VDP)Pb<sub>2</sub>Br<sub>6</sub> showed about 0.85 eV smaller bandgap [Fig. 12(c)] than that of (4,4'-EDP)Pb<sub>2</sub>Br<sub>6</sub>. Furthermore, (4,4'-VDP)Pb<sub>2</sub>Br<sub>6</sub> clearly showed photocurrent [Fig. 12(d)] and much better photoconductivity [Fig. 12(e)] compared with (4,4'-EDP)Pb<sub>2</sub>Br<sub>6</sub>.

#### III. SUMMARY AND OUTLOOK

Low-dimensional organic/inorganic hybrid perovskites (OIHPs) combine individual properties of organic molecules and inorganics into a single material system with unique and tunable features, thereby opening more possibilities for the design and development of advanced functional materials for a variety of applications (particularly optoelectronics). While most efforts have been dedicated to the design and synthesis of functional organics and different inorganic components to gain desirable functionalities, tuning the interactions in low-dimensional OIHPs, in particular, the non-covalent interactions between the organic cations have gained increasing amount of attention. Such non-covalent interactions can significantly influence a number of important properties of the low-dimensional OIHPs, such as dielectric confinement, bandgap, photoluminescence, quantum efficiency, charge mobility, trap density, and stability. Importantly, the analysis of crystal structures of low-dimensional OIHPs offers direct

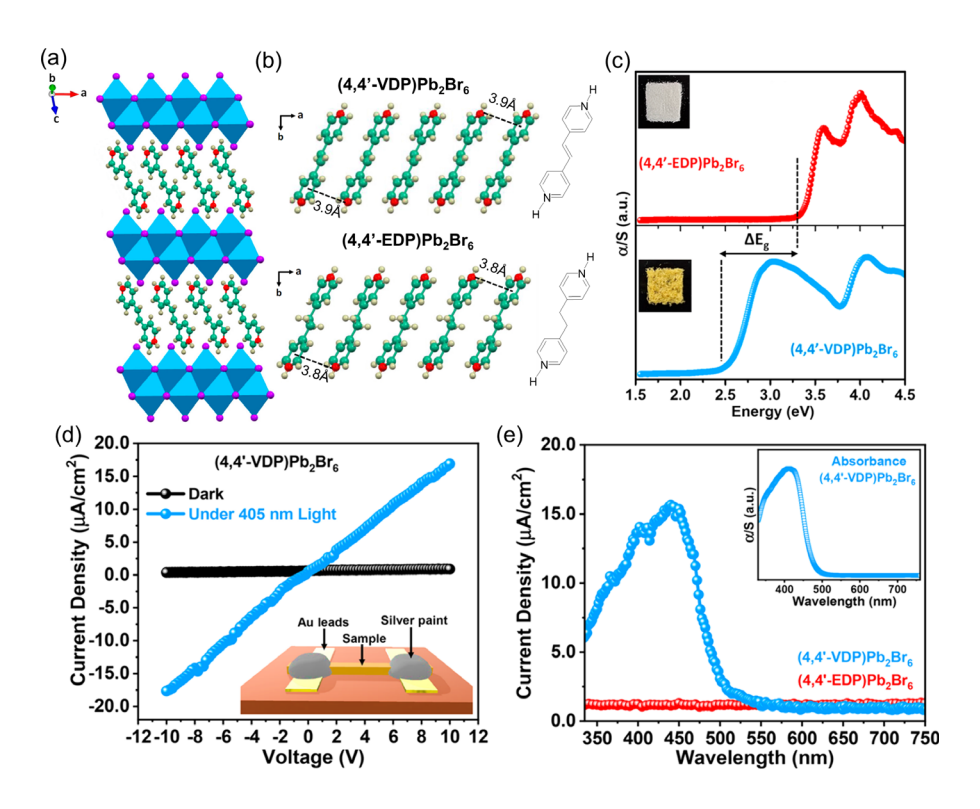


FIG. 12. (a) Crystal structure of (4,4'-VDP)Pb2Br6 obtained from single-crystal XRD at room temperature. (b) Comparison of 4,4'-VDP cations and 4,4'-EDP cations stacked in their individual single crystal 1D perovskites. (c) Ultraviolet-visible absorption spectra of (4,4'-VDP)Pb2Br6 (bottom) and (4,4'-EDP)Pb<sub>2</sub>Br<sub>6</sub> (top) polycrystals. The optical images of both samples under ambient light are shown in the insets of the corresponding panels. (d) Current-density-voltage (J-V) scan of a (4,4'-VDP)Pb2Br6 device in the dark and when illuminated by a 405 nm LED with a power of 20 mW/cm<sup>2</sup>. The inset shows the schematic of the device being tested. (e) Wavelength-dependent photoresponse of (4,4'-VDP)Pb2Br6 and (4,4'-EDP)Pb<sub>2</sub>Br<sub>6</sub> single crystals, under an applied bias of 50 V. The inset shows the optical absorption spectrum of (4,4'-VDP)Pb<sub>2</sub>Br<sub>6</sub>. Adapted with permission from Sheikh et al., J. Phys. Chem. Lett. 14, 1870 (2023). Copyright 2023 ACS.

evidence to understand these non-covalent interactions and to develop the structure–property relationship. Such fundamental insights and relationships will facilitate engineering approaches in which noncovalent interactions are leveraged for optoelectronic applications of low-dimensional OIHPs.

We focus on  $\pi$ -effect interactions in this perspective with a few selected examples; however, there are several other  $\pi$ -effect interactions that have not been actively explored, such as  $\pi$  donor-acceptor interactions and anion –  $\pi$  interactions. Since the impacts of these  $\pi$ effect interactions on the physical properties of organic molecules and materials have been widely investigated, 71-74 it is expected that further incorporation of previously unexplored interactions into lowdimensional OIHPs will open more avenues to explore. For example, the  $\pi$  donor-acceptor interaction is a strong non-covalent interaction that can reduce the distance between two involved species;<sup>73</sup> if this  $\pi$ donor-acceptor interaction were successfully implemented in low 2D OIHPs, the reduced distance among organic cations in 2D perovskites could enhance the stability and charge transfer properties of 2D perovskites. Only the  $\pi$  donor–acceptor interaction between organic cations and intercalated organic molecules has been employed to date, which has enabled reductions in the exciton binding energies for this subset of 2D perovskite systems.<sup>75</sup> Further exploration of the design of organic cations is still needed to fully understand and control the optoelectronic/physical properties of low-dimensional perovskites that originate in the  $\pi$  donor–acceptor interactions.

At this point, most studies of non-covalent interactions involving  $\pi$ -effects in low-dimensional OIHPs have been focused on the impact of such interactions on the crystal structures, phase formation, and optoelectronic properties. With stronger  $\pi$ -effect interactions, the low-dimensional phase is more stable, and the formation energy of the

low-dimensional phase could be tuned by adjusting the  $\pi$ -effect interaction. Stronger  $\pi$ – $\pi$  stacking would improve the charge transport and affect the nucleation of low-dimensional perovskites during the film formation process. However, there are other important topics, such as mechanical properties, thermal conductivity, and defect formation mechanisms (including point defects, line defects, and dislocations), all of which are worth further study. For example, Kim et al. recently discovered a chiral phonon activated spin Seebeck effect in chiral 2D perovskites;<sup>76</sup> the 2D perovskites in their work contained a chiral cation structurally similar to PEA. The  $\pi$ -effects together with other interactions, such as hydrogen bonding, would likely affect the distortion of the inorganic octahedra and further impact the chirality transfer from organic cations to the bulk perovskites, as Jana et al. demonstrated. Therefore, the spintronic properties might be tuned by adjusting the  $\pi$ -effect interactions. Given the vast design space of organic cations and inorganics, and various non-covalent interactions, we anticipate that more interesting low-dimensional OIHPs will emerge in the future, facilitated by further understanding of structure-property relationships. Finally, please note that there are many other lowdimensional perovskites that have employed large organic cations with  $\pi$  systems (e.g., aromatics); it is unclear whether the putative  $\pi$ -effect interactions play important roles in the structures and properties of these perovskites; thus, we strongly encourage further investigation and exploration of  $\pi$ -effect interactions in low-dimensional perovskites.

#### **ACKNOWLEDGMENTS**

This work was partially supported by the National Science Foundation (No. CHE-2154791).

## AUTHOR DECLARATIONS Conflict of Interest

The authors have no conflicts to disclose.

#### **Author Contributions**

**Liang Yan:** Writing – original draft (equal). **Camryn J. Gloor:** Writing – review & editing (supporting). **Andrew M. Moran:** Writing – review & editing (supporting). **Wei You:** Writing – original draft (equal); Writing – review & editing (equal).

#### DATA AVAILABILITY

Data sharing is not applicable to this article as no new data were created or analyzed in this study.

#### REFERENCES

- <sup>1</sup>M. Ahmadi, T. Wu, and B. Hu, Adv. Mater. 29(41), 1605242 (2017).
- <sup>2</sup>W. Shao, S. Yang, K. Wang, and L. Dou, J. Phys. Chem. Lett. **14**, 2034 (2023).
- <sup>3</sup>Y. Zhou and M. Saliba, ACS Energy Lett. **6**(8), 2750 (2021).
- <sup>4</sup>A. Kumar Jena, A. Kulkarni, and T. Miyasaka, Chem. Rev. 119(5), 3036 (2019).
- <sup>5</sup>D. Duan, C. Ge, M. Z. Rahaman, C.-H. Lin, Y. Shi, H. Lin, H. Hu, and T. Wu, NPG Asia Mater. 15(1), 8 (2023).
- <sup>6</sup>J. Almutlaq, J. Yin, O. F. Mohammed, and O. M. Bakr, J. Phys. Chem. Lett. <u>9</u>(14), 4131 (2018).
- <sup>7</sup>C. Zhou, L.-J. Xu, S. Lee, H. Lin, and B. Ma, Adv. Opt. Mater. **9**(18), 2001766 (2021).
- <sup>8</sup>j.-T. Lin, C.-C. Liao, C.-S. Hsu, D.-G. Chen, H.-M. Chen, M.-K. Tsai, P.-T. Chou, and C.-W. Chiu, J. Am. Chem. Soc. **141**(26), 10324 (2019).
- <sup>9</sup>B. Cheng, T.-Y. Li, P. Maity, P.-C. Wei, D. Nordlund, K.-T. Ho, D.-H. Lien, C.-H. Lin, R.-Z. Liang, X. Miao, I. A. Ajia, J. Yin, D. Sokaras, A. Javey, I. S. Roqan, O. F. Mohammed, and J.-H. He, Commun. Phys. 1(1), 80 (2018).
- <sup>10</sup>H. Li, X. Wang, T. Zhang, X. Gong, Q. Sun, H. Pan, Y. Shen, S. Ahmad, and M. Wang, Adv. Funct. Mater. 29(30), 1903293 (2019).
- <sup>11</sup>C. C. Boyd, R. Cheacharoen, T. Leijtens, and M. D. McGehee, Chem. Rev. 119(5), 3418 (2019).
- <sup>12</sup>G. Wu, R. Liang, M. Ge, G. Sun, Y. Zhang, and G. Xing, Adv. Mater. 34(8), 2105635 (2022).
- <sup>13</sup>X. Zhao, T. Liu, and Y.-L. Loo, Adv. Mater. 34(3), 2105849 (2022).
- <sup>14</sup>W. A. Dunlap-Shohl, Y. Zhou, N. P. Padture, and D. B. Mitzi, Chem. Rev. 119(5), 3193 (2019).
- <sup>15</sup>R. Lyu, C. E. Moore, T. Liu, Y. Yu, and Y. Wu, J. Am. Chem. Soc. **143**(32), 12766 (2021).
- <sup>16</sup>B. Saparov and D. B. Mitzi, Chem. Rev. 116(7), 4558 (2016).
- <sup>17</sup>X. Li, J. M. Hoffman, and M. G. Kanatzidis, Chem. Rev. **121**(4), 2230 (2021).
- <sup>18</sup>E. A. Meyer, R. K. Castellano, and F. Diederich, Angew. Chem., Int. Ed. 42(11), 1210 (2003).
- <sup>19</sup>J. Hu, I. W. H. Oswald, H. Hu, S. J. Stuard, M. M. Nahid, L. Yan, Z. Chen, H. Ade, J. R. Neilson, and W. You, ACS Mater. Lett. 1(1), 171 (2019).
- <sup>20</sup>J. Hu, I. W. H. Oswald, S. J. Stuard, M. M. Nahid, N. Zhou, O. F. Williams, Z. Guo, L. Yan, H. Hu, Z. Chen, X. Xiao, Y. Lin, Z. Yang, J. Huang, A. M. Moran, H. Ade, J. R. Neilson, and W. You, Nat. Commun. 10(1), 1276 (2019).
- <sup>21</sup>D. B. Mitzi, D. R. Medeiros, and P. R. L. Malenfant, Inorg. Chem. 41(8), 2134 (2002).
- <sup>22</sup>T. Sheikh, S. Maqbool, P. Mandal, and A. Nag, Angew. Chem., Int. Ed. **60**(33), 18265 (2021).
- <sup>23</sup>T. Sheikh, G. M. Anilkumar, T. Das, A. Rahman, S. Chakraborty, and A. Nag, J. Phys. Chem. Lett. **14**, 1870 (2023).
- <sup>24</sup>Z. Xu and D. B. Mitzi, Chem. Mater. **15**(19), 3632 (2003).
- <sup>25</sup>L. Yan, J. Hu, N. Zhou, A. M. Moran, and W. You, Sol. RRL 4(1), 1900374 (2020).
- <sup>26</sup>L. Yan, M. K. Jana, P. C. Sercel, D. B. Mitzi, and W. You, J. Am. Chem. Soc. 143(43), 18114 (2021).

- <sup>27</sup>F. Zhang, D. H. Kim, H. Lu, J.-S. Park, B. W. Larson, J. Hu, L. Gao, C. Xiao, O. G. Reid, X. Chen, Q. Zhao, P. F. Ndione, J. J. Berry, W. You, A. Walsh, M. C. Beard, and K. Zhu, J. Am. Chem. Soc. 141, 5972 (2019).
- <sup>28</sup>K. Jemli, P. Audebert, L. Galmiche, G. Trippé-Allard, D. Garrot, J.-S. Lauret, and E. Deleporte, ACS Appl. Mater. Interfaces 7(39), 21763 (2015).
- <sup>29</sup>L. Yan, J. Hu, Z. Guo, H. Chen, M. F. Toney, A. M. Moran, and W. You, ACS Appl. Mater. Interfaces 10(39), 33187 (2018).
- <sup>30</sup>G. Long, C. Jiang, R. Sabatini, Z. Yang, M. Wei, L. N. Quan, Q. Liang, A. Rasmita, M. Askerka, G. Walters, X. Gong, J. Xing, X. Wen, R. Quintero-Bermudez, H. Yuan, G. Xing, X. R. Wang, D. Song, O. Voznyy, M. Zhang, S. Hoogland, W. Gao, Q. Xiong, and E. H. Sargent, Nat. Photonics 12(9), 528 (2018).
- <sup>31</sup>K. Chondroudis and D. B. Mitzi, Chem. Mater. **11**(11), 3028 (1999).
- <sup>32</sup>D. B. Mitzi, K. Chondroudis, and C. R. Kagan, Inorg. Chem. 38(26), 6246 (1999).
- <sup>53</sup>j. V. Passarelli, D. J. Fairfield, N. A. Sather, M. P. Hendricks, H. Sai, C. L. Stern, and S. I. Stupp, J. Am. Chem. Soc. 140(23), 7313 (2018).
- <sup>34</sup>C. Liu, W. Huhn, K.-Z. Du, A. Vazquez-Mayagoitia, D. Dirkes, W. You, Y. Kanai, D. B. Mitzi, and V. Blum, Phys. Rev. Lett. **121**(14), 146401 (2018).
- 35Y. Gao, E. Shi, S. Deng, S. B. Shiring, J. M. Snaider, C. Liang, B. Yuan, R. Song, S. M. Janke, A. Liebman-Peláez, P. Yoo, M. Zeller, B. W. Boudouris, P. Liao, C. Zhu, V. Blum, Y. Yu, B. M. Savoie, L. Huang, and L. Dou, Nat. Chem. 11(12), 1151 (2019).
- <sup>36</sup>C. Ortiz-Cervantes, P. I. Román-Román, J. Vazquez-Chavez, M. Hernández-Rodríguez, and D. Solis-Ibarra, Angew. Chem., Int. Ed. 57(42), 13882 (2018).
- <sup>37</sup>Akriti, S. Zhang, Z.-Y. Lin, E. Shi, B. P. Finkenauer, Y. Gao, A. J. Pistone, K. Ma, B. M. Savoie, and L. Dou, Adv. Mater. 33(51), 2105183 (2021).
- <sup>38</sup>B. P. Dimitrijević, S. Z. Borozan, and S. D. Stojanović, RSC Adv. 2(33), 12963 (2012).
- <sup>39</sup>J. Hernández-Trujillo, F. Colmenares, G. Cuevas, and M. Costas, Chem. Phys. Lett. 265(3), 503 (1997).
- 40 E. M. Cabaleiro-Lago and J. Rodríguez-Otero, ACS Omega 3(8), 9348 (2018).
- <sup>41</sup>M. Nishio, Phys. Chem. Chem. Phys. **13**(31), 13873 (2011).
- <sup>42</sup>J. Shi, Y. Gao, X. Gao, Y. Zhang, J. Zhang, X. Jing, and M. Shao, Adv. Mater. 31(37), 1901673 (2019).
- <sup>43</sup>M. Dyksik, S. Wang, W. Paritmongkol, D. K. Maude, W. A. Tisdale, M. Baranowski, and P. Plochocka, J. Phys. Chem. Lett. 12(6), 1638 (2021).
- 44Y.-Q. Zhao, Q.-R. Ma, B. Liu, Z.-L. Yu, J. Yang, and M.-Q. Cai, Nanoscale 10(18), 8677 (2018).
- <sup>45</sup>J. Byun, H. Cho, C. Wolf, M. Jang, A. Sadhanala, R. H. Friend, H. Yang, and T.-W. Lee, Adv. Mater. 28(34), 7515 (2016).
- <sup>46</sup>X. Zhang, G. Wu, W. Fu, M. Qin, W. Yang, J. Yan, Z. Zhang, X. Lu, and H. Chen, Adv. Energy Mater. 8(14), 1702498 (2018).
- <sup>47</sup>I. C. Smith, E. T. Hoke, D. Solis-Ibarra, M. D. McGehee, and H. I. Karunadasa, Angew. Chem., Int. Ed. 53(42), 11232 (2014).
- 48 M. O. Sinnokrot, E. F. Valeev, and C. D. Sherrill, J. Am. Chem. Soc. 124(36), 10887 (2002).
- <sup>49</sup>C. A. Hunter and J. K. M. Sanders, J. Am. Chem. Soc. **112**(14), 5525 (1990).
- 50 B. W. Hopkins and G. S. Tschumper, J. Phys. Chem. A 108(15), 2941 (2004).
- <sup>51</sup>M. O. Sinnokrot and C. D. Sherrill, J. Phys. Chem. A **110**(37), 10656 (2006).
- <sup>52</sup>S. E. Wheeler and K. N. Houk, J. Am. Chem. Soc. **130**(33), 10854 (2008).
- <sup>53</sup>K.-Z. Du, Q. Tu, X. Zhang, Q. Han, J. Liu, S. Zauscher, and D. B. Mitzi, Inorg. Chem. 56(15), 9291 (2017).
- 54C. Janiak, J. Chem. Soc., Dalton Trans. 2000(21), 3885.
- 55Y. Gao, Z. Wei, P. Yoo, E. Shi, M. Zeller, C. Zhu, P. Liao, and L. Dou, J. Am. Chem. Soc. 141(39), 15577 (2019).
- <sup>56</sup>A. Liang, Y. Gao, R. Asadpour, Z. Wei, B. P. Finkenauer, L. Jin, J. Yang, K. Wang, K. Chen, P. Liao, C. Zhu, L. Huang, B. W. Boudouris, M. A. Alam, and L. Dou, J. Am. Chem. Soc. 143(37), 15215 (2021).
- 57T. Matsushima, S. Hwang, A. S. D. Sandanayaka, C. Qin, S. Terakawa, T. Fujihara, M. Yahiro, and C. Adachi, Adv. Mater. 28(46), 10275 (2016).
- <sup>58</sup>C. R. Patrick and G. S. Prosser, Nature **187**, 1021 (1960).
- 59G. W. Coates, A. R. Dunn, L. M. Henling, D. A. Dougherty, and R. H. Grubbs, Angew. Chem., Int. Ed. Engl. 36(3), 248 (1997).
- <sup>60</sup>G. W. Coates, A. R. Dunn, L. M. Henling, J. W. Ziller, E. B. Lobkovsky, and R. H. Grubbs, J. Am. Chem. Soc. **120**(15), 3641 (1998).

- <sup>61</sup>C. Dai, P. Nguyen, T. B. Marder, T. B. Marder, A. J. Scott, W. Clegg, C. Viney, and C. Viney, Chem. Commun. 1999(24), 2493.
- 62 F. Ponzini, R. Zagha, K. Hardcastle, and J. S. Siegel, Angew. Chem., Int. Ed. **39**(13), 2323 (2000).
- 63W. J. Feast, P. W. Lövenich, H. Puschmann, and C. Taliani, Chem. Commun. 2001(5), 505.
- 64 N. M. D. Brown and F. L. Swinton, J. Chem. Soc., Chem. Commun. 1974(19), 770.
- 65J. H. Williams, Acc. Chem. Res. 26(11), 593 (1993).
- 66 T. Glaser, C. Müller, M. Sendner, C. Krekeler, O. E. Semonin, T. D. Hull, O. Yaffe, J. S. Owen, W. Kowalsky, A. Pucci, and R. Lovrinčić, J. Phys. Chem. Lett. 6(15), 2913 (2015).
- 67Q. Tu, I. Spanopoulos, E. S. Vasileiadou, X. Li, M. G. Kanatzidis, G. S. Shekhawat, and V. P. Dravid, ACS Appl. Mater. Interfaces 12(18), 20440 (2020).
- <sup>68</sup>H. W. Tam, T. L. Leung, W. Sun, F. Liu, C. Ma, K. Sing Wong, I. Lončarić, L. Grisanti, J. Ovčar, Ž. Skoko, J. Popović, and A. B. Djurišić, J. Mater. Chem. C 8, 11052 (2020).

- 69 A. Subha Mahadevi and G. N. Sastry, Chem. Rev. 113(3), 2100 (2013).
- 70 D. A. Dougherty, Acc. Chem. Res. 46(4), 885 (2013).
- <sup>71</sup>J. C. Ma and D. A. Dougherty, Chem. Rev. **97**(5), 1303 (1997).
- 72B. L. Schottel, H. T. Chifotides, and K. R. Dunbar, Chem. Soc. Rev. 37(1), 68 (2008).

  73 A. Das and S. Ghosh, Angew. Chem., Int. Ed. 53(8), 2038 (2014).
- <sup>74</sup>H. A. Bent, Chem. Rev. **68**(5), 587 (1968).
- <sup>75</sup>J. V. Passarelli, C. M. Mauck, S. W. Winslow, C. F. Perkinson, J. C. Bard, H. Sai, K. W. Williams, A. Narayanan, D. J. Fairfield, M. P. Hendricks, W. A. Tisdale, and S. I. Stupp, Nat. Chem. 12(8), 672 (2020).
- <sup>76</sup>K. Kim, E. Vetter, L. Yan, C. Yang, Z. Wang, R. Sun, Y. Yang, A. H. Comstock, X. Li, J. Zhou, L. Zhang, W. You, D. Sun, and J. Liu, Nat. Mater. **22**, 322 (2023).
- 77M. K. Jana, R. Song, H. Liu, D. R. Khanal, S. M. Janke, R. Zhao, C. Liu, Z. Valy Vardeny, V. Blum, and D. B. Mitzi, Nat. Commun. 11(1), 4699 (2020).